

Unsupervised Lightweight Single Object Tracking with UHP-SOT++

Zhiruo Zhou, *Student member, IEEE*, Hongyu Fu, *Student member, IEEE*, Suya You, and C.-C. Jay Kuo, *Fellow, IEEE*

Abstract—An unsupervised, lightweight and high-performance single object tracker, called UHP-SOT, was proposed by Zhou *et al.* recently. As an extension, we present an enhanced version and name it UHP-SOT++ in this work. Built upon the foundation of the discriminative-correlation-filters-based (DCF-based) tracker, two new ingredients are introduced in UHP-SOT and UHP-SOT++: 1) background motion modeling and 2) object box trajectory modeling. The main difference between UHP-SOT and UHP-SOT++ is the fusion strategy of proposals from three models (i.e., DCF, background motion and object box trajectory models). An improved fusion strategy is adopted by UHP-SOT++ for more robust tracking performance against large-scale tracking datasets. Our second contribution lies in an extensive evaluation of the performance of state-of-the-art supervised and unsupervised methods by testing them on four SOT benchmark datasets – OTB2015, TC128, UAV123 and LaSOT. Experiments show that UHP-SOT++ outperforms all previous unsupervised methods and several deep-learning (DL) methods in tracking accuracy. Since UHP-SOT++ has extremely small model size, high tracking performance, and low computational complexity (operating at a rate of 20 FPS on an i5 CPU even without code optimization), it is an ideal solution in real-time object tracking on resource-limited platforms. Based on the experimental results, we compare pros and cons of supervised and unsupervised trackers and provide a new perspective to understand the performance gap between supervised and unsupervised methods, which is the third contribution of this work.

Index Terms—Object tracking, online tracking, single object tracking, unsupervised tracking.

I. INTRODUCTION

VIDEO object tracking is one of the fundamental computer vision problems. It finds rich applications in video surveillance [1], autonomous navigation [2], robotics vision [3], etc. Given a bounding box on the target object at the first frame, a tracker has to predict object box locations and sizes for all remaining frames in online single object tracking (SOT) [4]. The performance of a tracker is measured by accuracy (higher success rate), robustness (automatic recovery from tracking loss), computational complexity and speed (a higher number of frames per second of FPS).

Zhiruo Zhou, Hongyu Fu and C.-C. Jay Kuo are with the Ming-Hsieh Department of Electrical and Computer Engineering, University of Southern California, CA, 90089-2564, USA (e-mails: zhiruozh@usc.edu, hongyufu@usc.edu and cckuo@sipi.usc.edu).

Suya You is with Army Research Laboratory, Adelphi, Maryland, USA (e-mail: suya.you.civ@army.mil).

Online trackers can be categorized into supervised and unsupervised ones [5]. Supervised trackers based on deep learning (DL) dominate the SOT field in recent years. Some of them use a pre-trained network such as AlexNet [6] or VGG [7] as the feature extractor and do online tracking with extracted deep features [8]–[12]. Others adopt an end-to-end optimized model which is trained by video datasets in an offline manner [13], [14] and could be adapted to video frames in an online fashion [15]–[18]. The tracking problem is formulated as a template matching problem in siamese trackers [13], [14], [19]–[23], which is popular because of its simplicity and effectiveness. One recent trend is to apply the Vision Transformer in visual tracking [24], [25].

Although DL trackers offer state-of-the-art tracking accuracy, they do have some limitations. First, a large number of annotated tracking video clips are needed in the training, which is a laborious and costly task. Second, they demand large memory space to store the parameters of deep networks due to large model sizes. Third, the high computational power requirement hinders their applications in resource-limited devices such as drones or mobile phones. Fourth, DL trackers need to be trained with video samples of diverse content. Their capability in handling unseen objects appears to be limited, which will be illustrated in the experimental section. In contrast with DL trackers, unsupervised trackers are attractive since they do not need annotated boxes to train trackers. They are favored in real-time tracking on resource-limited devices because of lower power consumption.

Advanced unsupervised SOT methods often use discriminative correlation filters (DCF). They were investigated between 2010 and 2018 [9], [26]–[32]. DCF trackers conduct dense sampling around the object box and solve a regression problem to learn a template for similarity matching. Under the periodic sample assumption, matching can be conducted very fast in the Fourier domain. Spatial-temporal regularized correlation filters (STRCF) [32] adds spatial-temporal regularization to template update and performs favorably against other DCF trackers [8], [33].

As deep neural networks (DNNs) get popular in recent years, there is an increasing interest in learning DNN-based object tracking models from offline videos without annotations. For example, UDT+ [34] and LUDT [35] investigated cycle learning in video, in which networks are trained to track forward and backward with con-

sistent object proposals. ResPUL [36] mined positive and negative samples from unlabeled videos and leveraged them for supervised learning in building spatial and temporal correspondence. These unsupervised deep trackers reveal a promising direction in exploiting offline videos without annotations. Yet, they are limited in performance. Furthermore, they need the pre-training effort. In contrast, no pre-training on offline datasets is needed in our unsupervised tracker.

Despite the above-mentioned developments in unsupervised trackers, there is a significant performance gap between unsupervised DCF trackers and supervised DL trackers. It is attributed to the limitations of DCF trackers such as failure to recover from tracking loss and inflexibility in object box adaptation. An unsupervised tracker, called UHP-SOT (Unsupervised High-Performance Single Object Tracker), was recently proposed in [37] to address the issues. UHP-SOT used STRCF as the baseline and incorporated two new modules – background motion modeling and trajectory-based object box prediction. A simple fusion rule was adopted by UHP-SOT to integrate proposals from three modules into the final one. UHP-SOT has the potential to recover from tracking loss and offer flexibility in object box adaptation. UHP-SOT outperforms all previous unsupervised single object trackers and narrows down the gap between unsupervised and supervised trackers. It achieves comparable performance against DL trackers on small-scale datasets such as TB-50 and TB-100 (or OTB 2015) [38].

This work is an extension of UHP-SOT with new contributions. First, the fusion strategies in UHP-SOT and UHP-SOT++ are different. The fusion strategy in UHP-SOT was simple and ad hoc. UHP-SOT++ adopts a fusion strategy that is more systematic and well justified. It is applicable to both small- and large-scale datasets with more robust and accurate performance. Second, this work conducts more extensive experiments on four object tracking benchmarks (i.e., OTB2015, TC128, UAV123 and LaSOT) while only experimental results on OTB2015 were reported for UHP-SOT in [37]. New experimental evaluations demonstrate that UHP-SOT++ outperforms all previous unsupervised SOT methods (including UHP-SOT) and achieves comparable results with DL methods on large-scale datasets. Since UHP-SOT++ has an extremely small model size, high tracking performance, and low computational complexity (operating at a rate of 20 FPS on an i5 CPU even without code optimization), it is ideal for real-time object tracking on resource-limited platforms. Third, we make thorough discussion on pros and cons of supervised and unsupervised trackers in this work. Besides quantitative evaluations, we provide a few exemplary sequences with qualitative analysis on strengths and weaknesses of UHP-SOT++ and its benchmarking methods.

The rest of this paper is organized as follows. Related work is reviewed in Sec. II. The UHP-SOT++ method is detailed in Sec. III. Experimental results are shown in Sec. IV. Further discussion is provided in Sec. V.

Concluding remarks are given in Sec. VI.

II. RELATED WORK

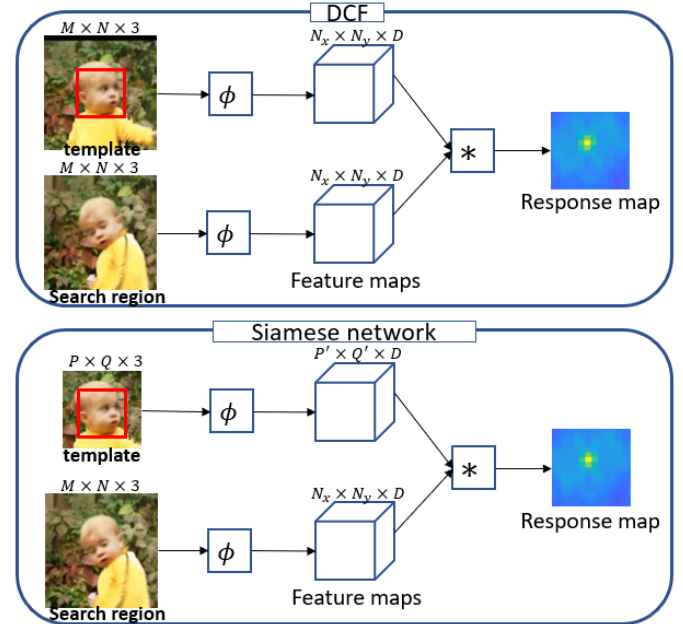


Fig. 1: Comparison of the inference structures of a DCF tracker and a siamese network tracker, where the red box denotes the object bounding box, ϕ is the feature extraction module and $*$ is the correlation operation.

A. DCF and Siamese Networks

Two representative single object trackers are reviewed and compared here. They are the DCF tracker and the siamese network tracker as shown in Fig. 1. The former is an unsupervised one while the latter is a supervised one based on DL. Both of them conduct template matching within a search region to generate the response map for object location. The matched template in the next frame is centered at the location that has the highest response.

In the DCF, the template size is the same as that of the search region so that the Fast Fourier Transform (FFT) could be used to speed up the correlation process. To learn the template, a DCF uses the initial object patch to obtain a linear template via regression in the Fourier domain:

$$\arg \min_{\mathbf{f}} \frac{1}{2} \left\| \sum_{d=1}^D \mathbf{x}^d * \mathbf{f}^d - \mathbf{y} \right\|^2, \quad (1)$$

where \mathbf{f} is the template to be determined, $\mathbf{x} \in \mathbb{R}^{N_x \times N_y \times D}$ is the spatial map of D features extracted from the object patch, $*$ is the feature-wise spatial convolution, and $\mathbf{y} \in \mathbb{R}^{N_x \times N_y}$ is a centered Gaussian-shaped map that serves as the regression label. Templates in DCFs tend to contain some background information. Furthermore, there exists boundary distortion caused by the 2D Fourier transform. To alleviate these side effects, it is

often to weigh the template with a window function to suppress background and image discontinuity.

In contrast, the template size in a siamese networks is more flexible and significantly smaller than the search region. Usually, the object box of the first frame serves as the template for the search in all later frames. The correlation is typically implemented by the convolution which runs fast on GPU. The shape and size of the predicted object bounding box are determined by the regional proposal network inside the siamese network.

B. Spatial-Temporal Regularized Correlation Filters (STRCF)

STRCF is a DCF-based tracker. It has an improved regression objective function using spatial-temporal regularization. The template is initialized at the first frame. Suppose that the object appearance at frame t is modeled by a template, denoted by \mathbf{f}_t , which will be used for similarity matching at frame $(t + 1)$. By modifying Eq. (1), STRCF updates its template at frame t by solving the following regression equation:

$$\arg \min_{\mathbf{f}} \left\{ \frac{1}{2} \left\| \sum_{d=1}^D \mathbf{x}_t^d * \mathbf{f}^d - \mathbf{y} \right\|^2 + \frac{1}{2} \sum_{d=1}^D \|\mathbf{w} \cdot \mathbf{f}^d\|^2 + \frac{\mu}{2} \|\mathbf{f} - \mathbf{f}_{t-1}\|^2 \right\} \quad (2)$$

where \mathbf{w} is the spatial weight on the template, \mathbf{f}_{t-1} is the template obtained from time $t - 1$, and μ is a constant regularization coefficient. We can interpret the three terms in Eq. (2) as follows. The first term is the standard regression objective function of a DCF. The second term imposes the spatial regularization. It gives more weights to features in the center region of a template in the matching process. The third term imposes temporal regularization for smooth appearance change.

To search for the box in frame $(t+1)$, STRCF correlates template \mathbf{f}_t with the search region and determines the new box location by finding the location that gives the highest response. Although STRCF can model the appearance change for general sequences, it suffers from overfitting. That is, it is not able to adapt to largely deformed objects quickly. Furthermore, it cannot recover from tracking loss. The template model, \mathbf{f} , is updated at every frame with a fixed regularization coefficient, μ , in standard STRCF.

Our UHP-SOT++ adopts STRCF as a building module. To address the above-mentioned shortcomings, we have some modification in our implementation. First, we skip updating \mathbf{f} if no obvious motion is observed. Second, a smaller μ is used when all modules agree with each other in prediction so that \mathbf{f} can adapt to the new appearance of largely deformed objects faster.

III. PROPOSED UHP-SOT++ METHOD

A. System Overview

There are three main challenges in SOT:

- 1) significant change of object appearance,

- 2) loss of tracking,

- 3) rapid variation of object's location and/or shape.

We propose a new tracker, UHP-SOT++, to address these challenges, As shown in Fig. 2, it consists of three modules:

- 1) appearance model update,
- 2) background motion modeling,
- 3) trajectory-based box prediction.

UHP-SOT++ follows the classic tracking-by-detection paradigm where the object is detected within a region centered at its last predicted location at each frame. The histogram of gradients (HOG) features as well as the color name (CN) [39] features are extracted to yield the feature map. We choose the STRCF tracker [32] as the baseline because of its efficient and effective appearance modeling and update. Yet, STRCF cannot handle the second and the third challenges well because it only focuses on the modeling of object appearance which could vary a lot across different frames. Generally, the high variety of object appearance is difficult to capture using a single model. Thus, we propose the second and the third modules in UHP-SOT++ to enhance its tracking accuracy. UHP-SOT++ operates in the following fashion. The baseline tracker gets initialized at the first frame. For the following frames, UHP-SOT++ gets proposals from all three modules and merges them into the final prediction based on a fusion strategy.

The STRCF tracker was already discussed in Sec. II-B. For the rest of this section, we will examine the background motion modeling module and the trajectory-based box prediction module in Secs. III-B and III-C, respectively. Finally, we will elaborate on the fusion strategy in Sec. III-D. Note that the fusion strategies of UHP-SOT and UHP-SOT++ are completely different.

B. Background Motion Modeling

We decompose the pixel displacement between adjacent frames (also called optical flow) into two types: object motion and background motion. Background motion is usually simpler, and it may be fit by a parametric model. Background motion estimation [40], [41] finds applications in video stabilization, coding and visual tracking. Here, we propose a 6-parameter model in form of

$$x_{t+1} = \alpha_1 x_t + \alpha_2 y_t + \alpha_0, \quad (3)$$

$$y_{t+1} = \beta_1 x_t + \beta_2 y_t + \beta_0, \quad (4)$$

where (x_{t+1}, y_{t+1}) and (x_t, y_t) are corresponding background points in frames $(t + 1)$ and t , respectively, and α_i and β_i , $i = 0, 1, 2$ are model parameters. With more than three pairs of corresponding points, we can determine the model parameters using the linear least-squares method. Usually, we choose a few salient points (e.g., corners) to build the correspondence. We apply the background model to the grayscale image $I_t(x, y)$ of

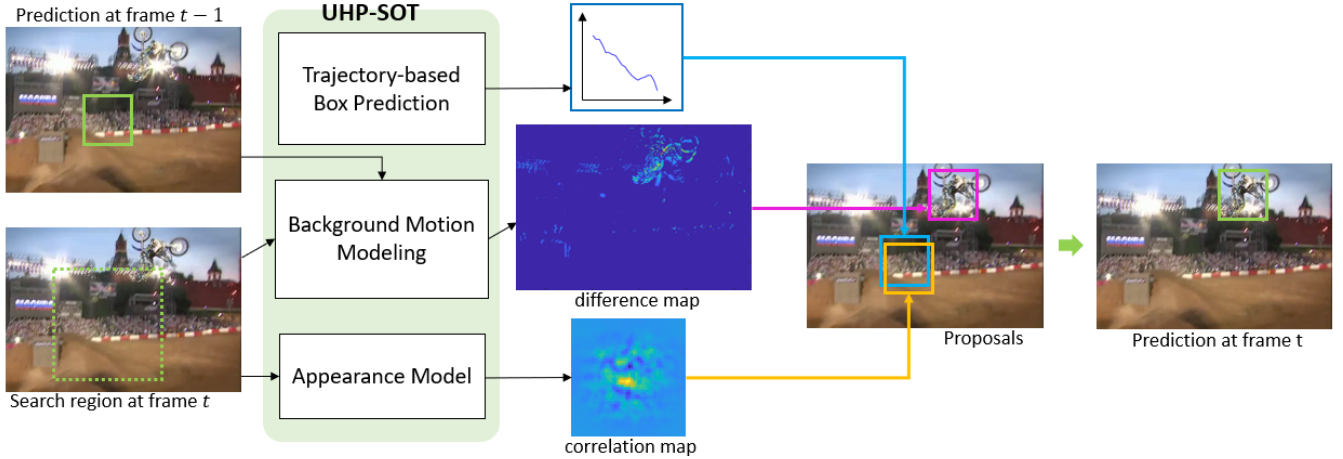


Fig. 2: The system diagram of the proposed UHP-SOT++ method. It shows one example where the object was lost at time $t - 1$ but gets retrieved at time t because the proposal from background motion modeling is accepted.

frame t to find the estimated $\hat{I}_{t+1}(x, y)$ of frame $(t + 1)$. Then, we can compute the difference map ΔI :

$$\Delta I = \hat{I}_{t+1}(x, y) - I_{t+1}(x, y), \quad (5)$$

which is expected to have small and large absolute values in the background and foreground regions, respectively. Thus, we can determine potential object locations. While DCF trackers exploit foreground correlation to locate the object, background modeling uses background correlation to eliminate background influence in object tracking. They complement each other. DCF trackers cannot recover from tracking loss easily since it does not have a global view of the scene. In contrast, our background modeling can find potential object locations by removing the background.

C. Trajectory-based Box Prediction

Given predicted box centers of the object of the last N frames, $\{(x_{t-N}, y_{t-N}), \dots, (x_{t-1}, y_{t-1})\}$, we calculate $N - 1$ displacement vectors $\{(\Delta x_{t-N+1}, \Delta y_{t-N+1}), \dots, (\Delta x_{t-1}, \Delta y_{t-1})\}$ and apply the principal component analysis (PCA) to them. To predict the displacement at frame t , we fit the first principal component using a line and set the second principal component to zero to remove noise. Then, the center location of the box at frame t can be written as

$$(\hat{x}_t, \hat{y}_t) = (x_{t-1}, y_{t-1}) + (\hat{\Delta x}_t, \hat{\Delta y}_t). \quad (6)$$

Similarly, we can estimate the width and the height of the box at frame t , denoted by (\hat{w}_t, \hat{h}_t) . Typically, the physical motion of an object has an inertia in motion trajectory and its size, and the box prediction process attempts to maintain the inertia. It contributes to better tracking performance in two ways. First, it removes small fluctuation of the box in its location and size. Second, when there is a rapid deformation of the target object, the appearance model alone cannot capture the shape change effectively. In contrast, the combination of

background motion modeling and the trajectory-based box prediction can offer a more satisfactory solution. For example, Fig. 3, shows a frame of the *diving* sequence in the upper-left subfigure, where the green and the magenta boxes are the ground truth and the result of UHP-SOT++, respectively. Although a DCF tracker can detect the size change by comparing correlation scores at five image resolutions, it cannot estimate the aspect ratio change properly. In contrast, as shown in the lower-left subfigure, the residual image after background removal in UHP-SOT++ reveals the object shape. By summing up absolute pixel values of the residual image horizontally and vertically and using a threshold to determine two ends of the box, we have

$$\hat{w} = x_{\max} - x_{\min}, \text{ and } \hat{h} = y_{\max} - y_{\min}. \quad (7)$$

Note that raw estimates may not be stable across different frames. Estimates that deviate much from the trajectory of $(\Delta w_t, \Delta h_t)$ are rejected to yield a robust and deformable box proposal.

D. Fusion Strategy

We have three box proposals for the target object at frame t : 1) B_{app} from the baseline STRCF tracker to capture appearance change, 2) B_{bgd} from the background motion predictor to eliminate unlikely object regions, and 3) B_{trj} from the trajectory predictor to maintain the inertia of the box position and size. A fusion strategy is needed to yield the final box location and size. We consider a couple of factors for its design.

1) *Proposal Quality*: There are three box proposals. The quality of each box proposal can be measured by: 1) object appearance similarity, and 2) robustness against the trajectory. We use a binary flag to indicate whether the quality of a proposal is good or not. As shown in Table I, the flag is set to one if a proposal keeps proper appearance similarity and is robust against trajectory. Otherwise, it is set to zero.

TABLE I: All tracking scenarios are classified into 8 cases in terms of the overall quality of proposals from three modules. The fusion strategy is set up for each scenario. The update rate is related the regularization coefficient, μ , that controls to which extent the appearance model should be updated.

$isGood_{app}$	$isGood_{trj}$	$isGood_{bgd}$	Proposal to take	Update rate
1	1	1	B_{app} or union of three	normal
1	1	0	B_{app} or B_{trj} or union of two	normal
1	0	1	B_{app} or B_{bgd} or union of two	normal
0	1	1	B_{trj} or B_{bgd} or union of two	normal or stronger
1	0	0	B_{app}	normal
0	1	0	B_{app} or B_{trj}	normal or stronger
0	0	1	B_{app} or B_{bgd}	normal or stronger
0	0	0	B_{app} or last prediction in case of occlusion	normal or weaker

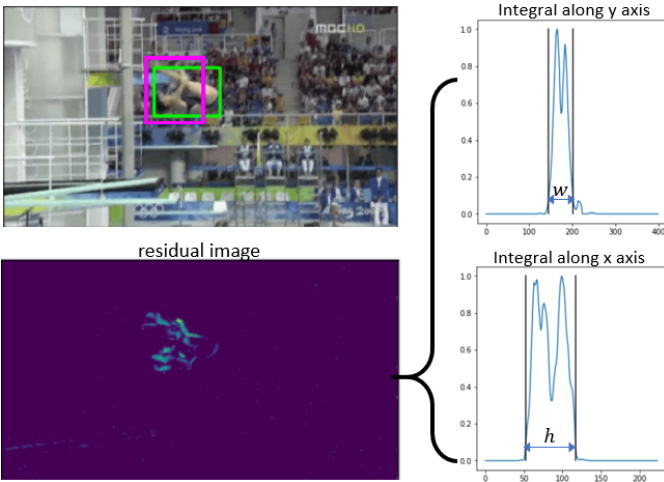


Fig. 3: Illustration of shape change estimation based on background motion model and trajectory-based box prediction, where the ground truth and our proposal are annotated in green and magenta, respectively.

For the first measure, we store two appearance models: the latest model, \mathbf{f}_{t-1} , and an older model, \mathbf{f}_i , $i \leq t-1$, where i is the last time instance where all three boxes have the same location. Model \mathbf{f}_i is less likely to be contaminated since it needs agreement from all modules. To check the reliability of the three proposals, we compute correlation scores for the following six pairs: $(\mathbf{f}_{t-1}, B_{app})$, $(\mathbf{f}_{t-1}, B_{trj})$, $(\mathbf{f}_{t-1}, B_{bgd})$, (\mathbf{f}_i, B_{app}) , (\mathbf{f}_i, B_{trj}) , and (\mathbf{f}_i, B_{bgd}) . They provide appearance similarity measures of the two previous models against the current three proposals. A proposal has good similarity if one of its correlation scores is higher than a threshold.

For the second measure, if B_{app} and B_{trj} have a small displacement (say, 30 pixels) from the last prediction, the move is robust. As to B_{bgd} , it often jumps around and, thus, is less reliable. However, if the standard deviations of its historical locations along the x -axis and y -axis are small enough (e.g., 30 pixels over the past 10 frames),

then they are reliable.

2) *Occlusion Detection*: We propose an occlusion detection strategy for color images, which is illustrated in Fig. 4. As occlusion occurs, we often observe a sudden drop in the similarity score and a rapid change on the averaged RGB color values inside the box. A drop is sudden if the mean over the past several frames is high while the current value is significantly lower. If this is detected, we keep the new prediction the same as the last predicted position since the new prediction is unreliable. We do not update the model for this frame either to avoid drifting and/or contamination of the appearance model.

3) *Rule-based Fusion*: Since each of the three proposals has a binary flag, all tracking scenarios can be categorized into 8 cases as shown in Fig. 5. We propose a fusion scheme for each case below.

- When all three proposals are good, their boxes are merged together as a minimum covering rectangle if they overlap with each other with IoU above a threshold. Otherwise, B_{app} is adopted.
- When two proposals are good, merge them if they overlap with each other with IoU above a threshold. Otherwise, the one with better robustness is adopted.
- When one proposal is good, adopt that one if it is B_{app} . Otherwise, that proposal is compared with B_{app} to verify its superiority by observing a higher similarity score or better robustness.
- When all proposals have poor quality, the occlusion detection process is conducted. The last prediction is adopted in case of occlusion. Otherwise, B_{app} is adopted.
- When other proposals outperform B_{app} , the regularization coefficient, μ , is adjusted accordingly for stronger update. Because this might reveal that the appearance model needs to be updated more to capture the new appearance.

The fusion rule is summarized in Table I. In most cases,

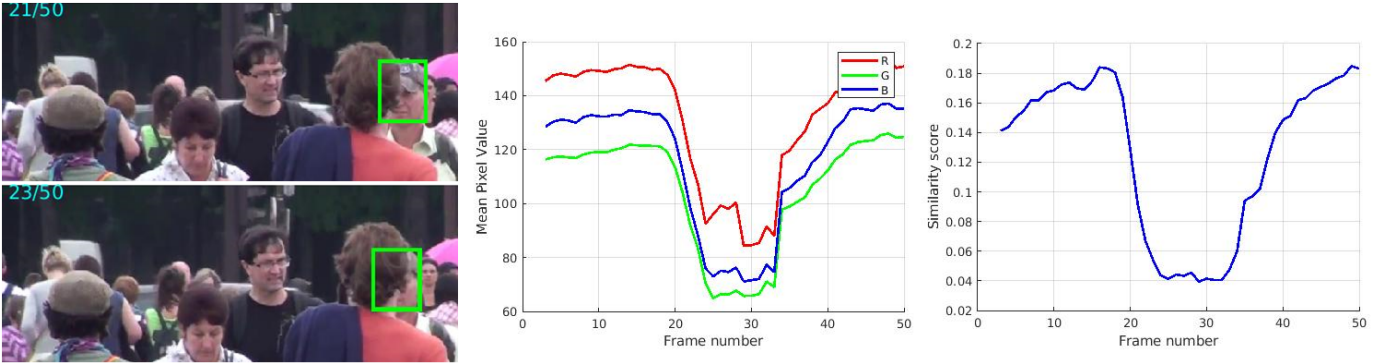


Fig. 4: Illustration of occlusion detection, where the green box shows the object location. The color information and similarity score could change rapidly if occlusion occurs.

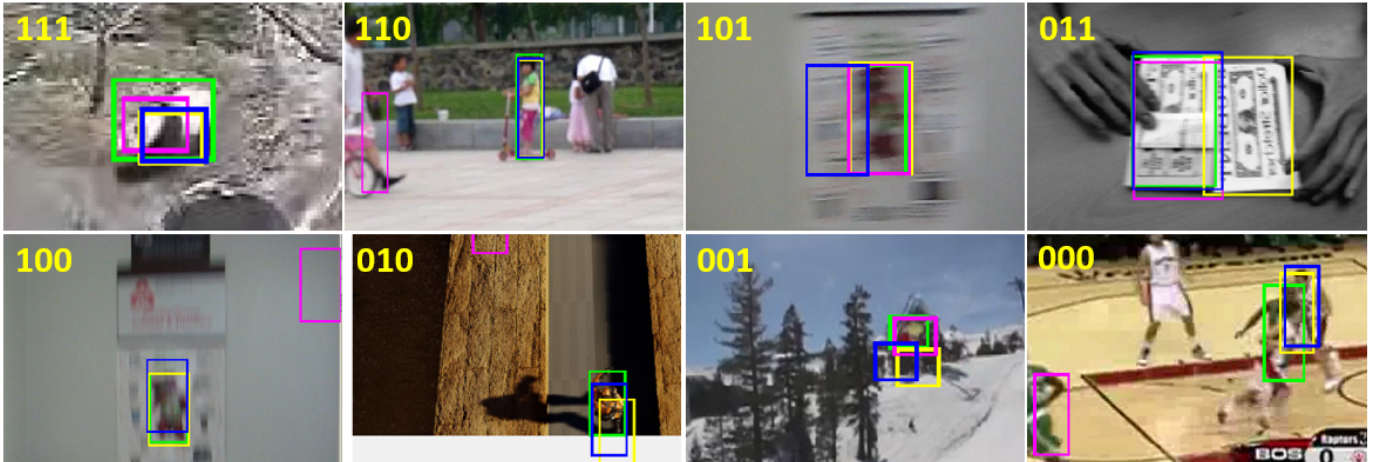


Fig. 5: An example of quality assessment of proposals, where the green box is the ground truth, and yellow, blue and magenta boxes are proposals from B_{app} , B_{trj} and B_{bgd} , respectively, and the bright yellow text on the top-left corner denotes the quality of three proposals ($isGood_{app}$, $isGood_{trj}$, $isGood_{bgd}$).

B_{app} is reliable and it will be chosen or merged with other proposals because the change is smooth between adjacent frames in the great majority of frames in a video clip.

IV. EXPERIMENTS

A. Experimental Set-up

To show the performance of UHP-SOT++, we compare it with several state-of-the-art unsupervised and supervised trackers on four single object tracking datasets. They are OTB2015 [38], TC128 [42], UAV123 [43] and LaSOT [44]. OTB2015 (also named OTB in short) and TC128, which contain 100 and 128 color or grayscale video sequences, respectively, are two widely used small-scale datasets. UAV123 is a larger one, which has 123 video sequences with more than 110K frames in total. Videos in UAV123 are captured by low-altitude drones. They are useful in the tracking test of small objects with a rapid change of viewpoints. LaSOT is the largest single object tracking dataset that targets at diversified object classes and flexible motion trajectories in longer sequences. It has one training set with dense annotation

for supervised trackers to learn and another test set for performance evaluation. The test set contains 280 videos of around 685K frames.

Performance evaluation is conducted using the ‘‘One Pass Evaluation (OPE)’’ protocol. The metrics include the precision plot (i.e., the distance of the predicted and actual box centers) and the success plot (i.e., overlapping ratios at various thresholds). The distance precision (DP) is measured at the 20-pixel threshold to rank different methods. The overlap precision is measured by the area-under-curve (AUC) score. We use the same hyperparameters as those in STRCF except for regularization coefficient, μ . If the appearance box is not chosen, STRCF sets $\mu = 15$ while UHP-SOT++ selects $\mu \in \{15, 10, 5, 0\}$. The smaller μ is, the stronger the update is. The number of previous frames for trajectory prediction is $N = 20$. The cutting threshold along the horizontal or vertical direction is set 0.1. The threshold for good similarity score is 0.08, and a threshold of 0.5 for IoU is adopted. UHP-SOT++ runs at 20 frames per second (FPS) on a PC equipped with an Intel(R) Core(TM) i5-9400F CPU. The speed data of other trackers are either from their original papers or benchmarks. Since no code optimization is

conducted, all reported speed data should be viewed as lower bounds for the corresponding trackers.

B. Ablation study

We compare different configurations of UHP-SOT++ on the TC128 dataset to investigate contributions from each module in Fig. 6. As compared with UHP-SOT, improvements on both DP and AUC in UHP-SOT++ come from the new fusion strategy. Under this strategy, the background motion modeling plays an more important role and it has comparable performance even without the trajectory prediction. Although the trajectory prediction module is simple, it contributes a lot to higher tracking accuracy and robustness as revealed by the performance improvement over the baseline STRCF.

More performance comparison between UHP-SOT++, UHP-SOT and STRCF is presented in Table II. As compared with STRCF, UHP-SOT++ achieves 1.8%, 6.2%, 6.7% and 6.8% gains in the success rate on OTB, TC128, UAV123 and LaSOT, respectively. As to the mean precision, it has an improvement of 1.2%, 6.9%, 7.2% and 10.4%, respectively. Except for OTB, UHP-SOT++ outperforms UHP-SOT in both the success rate and the precision. This is especially obvious for large-scale datasets. Generally, UHP-SOT++ has better tracking capability than UHP-SOT. Its performance drop in OTB is due to the tracking loss in three sequences; namely, *Bird2*, *Coupon* and *Freeman4*. They have complicated appearance changes such as severe rotation, background clutter and heavy occlusion. As shown in Fig. 7, errors at some key frames lead to total loss of the object, and the lost object cannot be easily recovered from motion. The trivial fusion strategy based on appearance similarity in UHP-SOT seems to work well on their key frames while the fusion strategy of UHP-SOT++ does not suppress wrong proposals properly since background clutters have stable motion and trajectories as well.

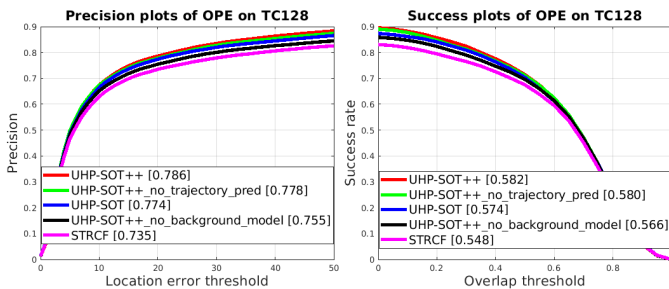


Fig. 6: The precision plot and the success plot of our UHP-SOT++ tracker with different configurations on the TC128 dataset, where the numbers inside the parentheses are the DP values and AUC scores, respectively.

C. Comparison with State-of-the-art Trackers

We compare the performance of UHP-SOT++ and several unsupervised trackers for the LaSOT dataset in



Fig. 7: Failure cases of UHP-SOT++ (in green) as compared to UHP-SOT (in red) on OTB2015.

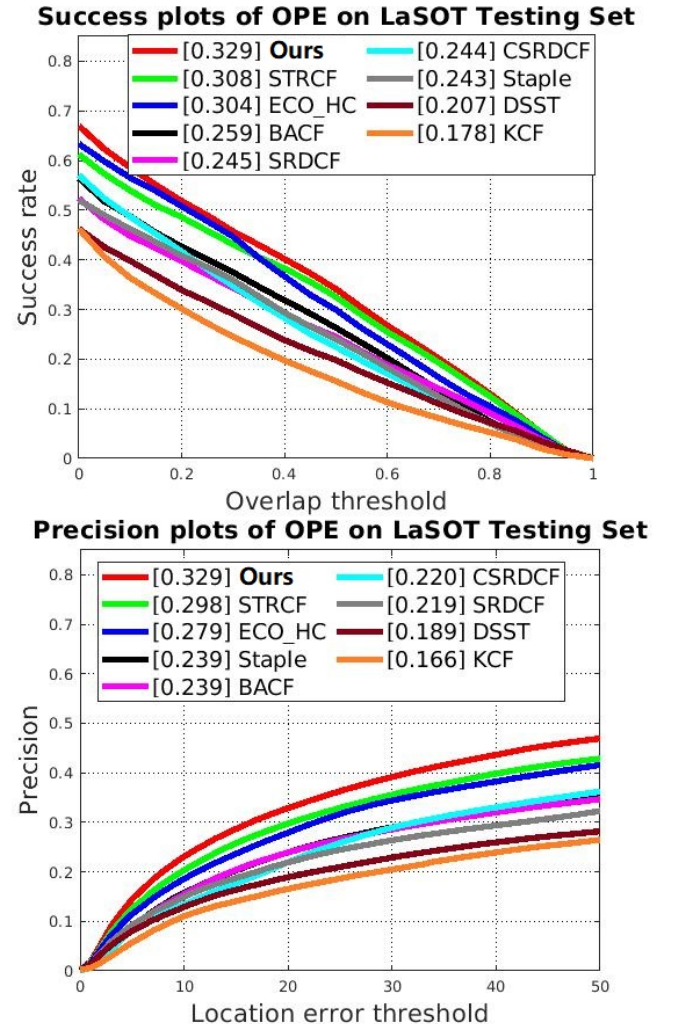


Fig. 8: The success plot and the precision plot of nine unsupervised tracking methods for the LaSOT dataset, where the numbers inside the parentheses are the overlap precision and the distance precision values, respectively.

TABLE II: Comparison of state-of-the-art supervised and unsupervised trackers on four datasets, where the performance is measure by the distance precision (DP) and the area-under-curve (AUC) score in percentage. The model size is measured by the memory required to store needed data such as the model parameters of pre-trained networks. The best unsupervised performance is highlighted. Also, S and P indicate Supervised and Pre-trained, respectively.

Trackers	Year	S	P	OTB2015		TC128		UAV123		LaSOT		FPS	Device	Model size (MB)
				DP	AUC	DP	AUC	DP	AUC	DP	AUC			
SiamRPN++ [14]	2019	✓	✓	91.0	69.2	-	-	84.0	64.2	49.3	49.5	35	GPU	206
ECO [8]	2017	✓	✓	90.0	68.6	80.0	59.7	74.1	52.5	30.1	32.4	10	GPU	329
UDT+ [34]	2019	×	✓	83.1	63.2	71.7	54.1	-	-	-	-	55	GPU	< 1
LU DT [35]	2020	×	✓	76.9	60.2	67.1	51.5	-	-	-	26.2	70	GPU	< 1
ResPUL [36]	2021	×	✓	-	58.4	-	-	-	-	-	-	-	GPU	> 6
ECO-HC [8]	2017	×	×	85.0	63.8	75.3	55.1	72.5	50.6	27.9	30.4	42	CPU	< 1
STRCF [32]	2018	×	×	86.6	65.8	73.5	54.8	67.8	47.8	29.8	30.8	24	CPU	< 1
UHP-SOT [37]	2021	×	×	90.9	68.9	77.4	57.4	71.0	50.1	31.1	32.0	23	CPU	< 1
UHP-SOT++	Ours	×	×	87.6	66.9	78.6	58.2	72.7	51.0	32.9	32.9	20	CPU	< 1

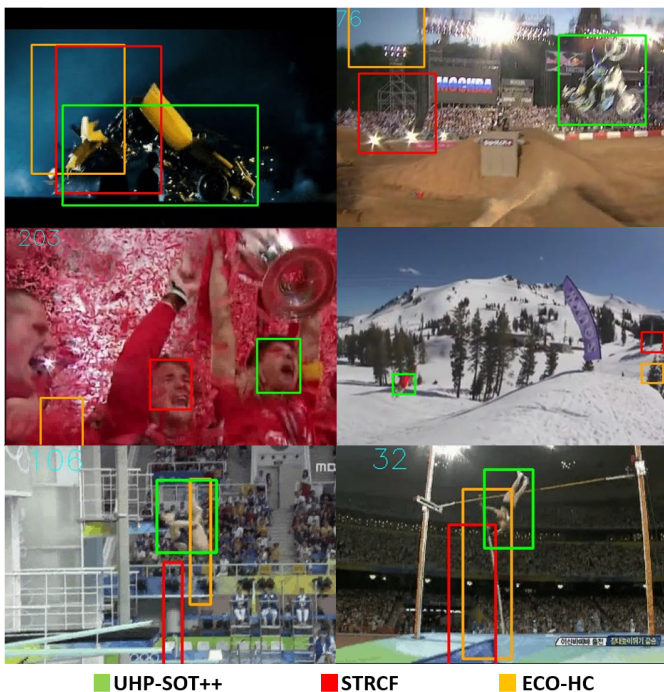


Fig. 9: Qualitative evaluation of three leading unsupervised trackers, where UHP-SOT++ offers a robust and flexible box prediction.

Fig. 8. The list of benchmarking methods includes ECO-HC [8], STRCF [32], CSR-DCF [45], SRDCF [33], Staple [30], KCF [27], DSST [29]. UHP-SOT++ outperforms other unsupervised methods by a large margin, which is larger than 0.02 in the mean scores of the success rate and the precision. Besides, its running speed is 20 FPS, which is comparable with that of the second runner STRCF (24 FPS) and the third runner (42 FPS)

based on experiments in OTB. With a small increase in computational and memory resources, UHP-SOT++ gains in tracking performance by adding object box trajectory and background motion modeling modules. Object boxes of three leading unsupervised trackers are visualized in Fig. 9 for qualitative performance comparison. As compared with other methods, the proposals of UHP-SOT++ offer a robust and flexible box prediction. They follow tightly with the object in both location and shape even under challenging scenarios such as motion blur and rapid shape change.

We compare the success rates of UHP-SOT++ and several supervised and unsupervised trackers against all four datasets in Fig. 10. Note that there are more benchmarking methods for OTB but fewer for TC128, UA123 and LaSOT since OTB is an earlier dataset. The supervised deep trackers under consideration include SiamRPN++ [14], ECO [8], C-COT [9], DeepSRDCF [33], HDT [5], SiamFC_3s [19], CFNet [31] and LCT [46]. Other deep trackers that have leading performance but are not likely to be used on resource-limited devices due to their extremely high complexity, such as transformer-based trackers [24], [25], are not included here. Although the performance of a tracker may vary from one dataset to the other due to different video sequences collected by each dataset, UHP-SOT++ is among the top three in all four datasets. This demonstrates the generalization capability of UHP-SOT++. Its better performance than ECO on LaSOT indicates a robust and effective update of the object model. Otherwise, it would degrade quickly with worse performance because of longer LaSOT sequences. Besides, its tracking speed of 20 FPS on CPU is faster than many deep trackers such as ECO (10 FPS), DeepSRDCF (0.2 FPS), C-COT (0.8 FPS) and HDT (2.7

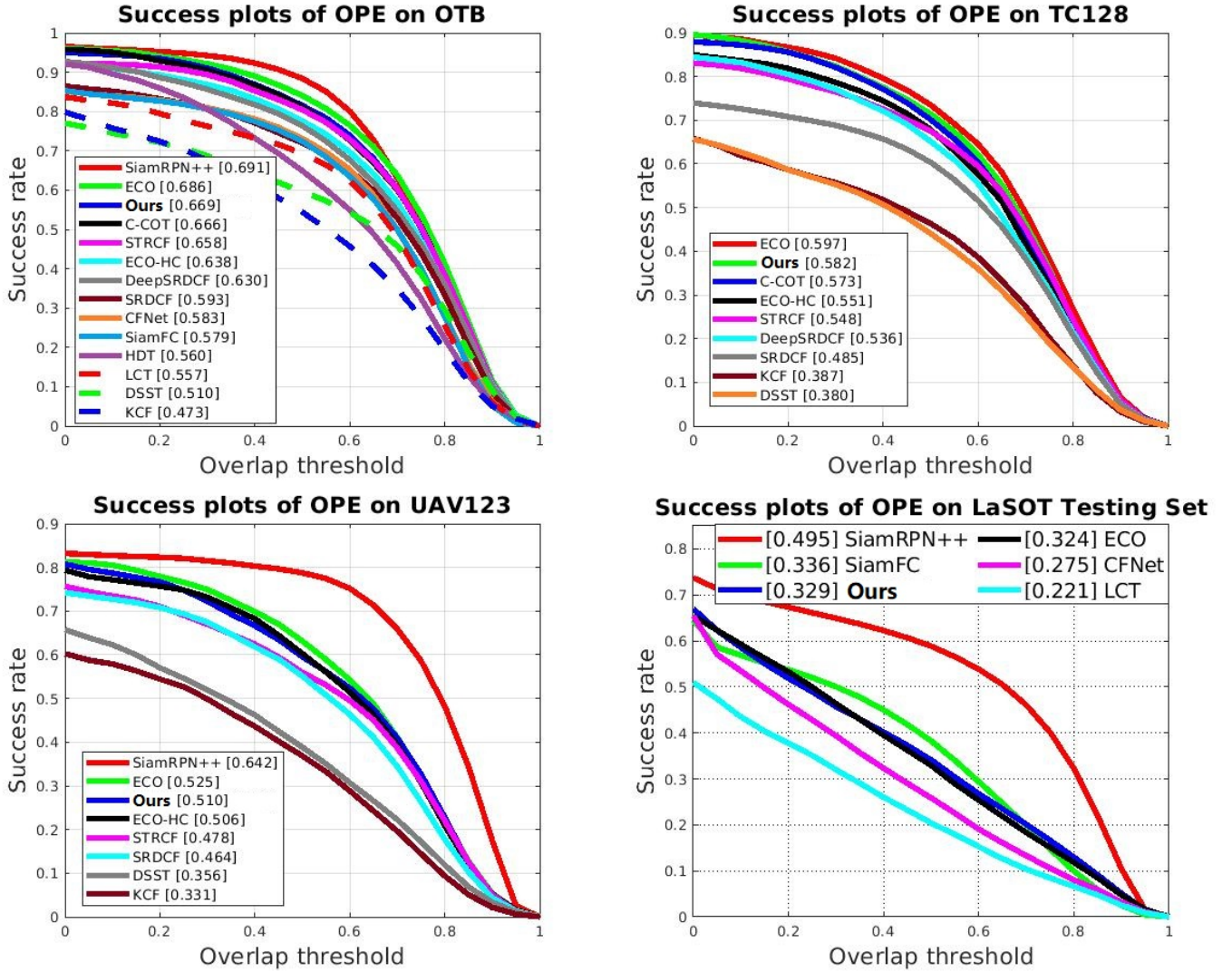


Fig. 10: The success plot comparison of UHP-SOT++ with several supervised and unsupervised tracking methods on four datasets, where only trackers with raw results published by authors are listed. For the LaSOT dataset, only supervised trackers are included for performance benchmarking in the plot since the success plot of unsupervised methods is already given in Fig. 8.

FPS).

In Table II, we further compare UHP-SOT++ with state-of-the-art unsupervised deep trackers UDT+ [34], LUDT [35] and ResPUL [36] in their AUC and DP values, running speeds and model sizes. Two leading supervised trackers SiamRPN++ and ECO in Fig. 10 are also included. It shows that UHP-SOT++ outperforms recent unsupervised deep trackers by a large margin. We should emphasize that deep trackers demand pre-training on offline datasets while UHP-SOT++ does not. In addition, UHP-SOT++ is attractive because of its lower memory requirement and near real-time running speed on CPUs. Although ECO-HC also provides a light-weight solution, there is a performance gap between UHP-SOT++ and ECO-HC. SiamRPN++ has the best tracking performance among all trackers, due to the merit of end-to-end optimized network

with auxiliary modules such as classification head and the region proposal network. Yet, its large model size and GPU hardware requirement limit its applicability in resource-limited devices such as mobile phones or drones. In addition, as an end-to-end optimized deep tracker, SiamRPN++ has the interpretability issue to be discussed later.

D. Attribute-based Study

To better understand the capability of different trackers, we analyze the performance variation under various challenging tracking conditions. These conditions can be classified into the following attributes: aspect ratio change (ARC), background clutter (BC), camera motion (CM), deformation (DEF), fast motion (FM), full occlusion (FOC), in-plane rotation (IPR), illumination variation (IV), low resolution (LR), motion blur (MB), oc-

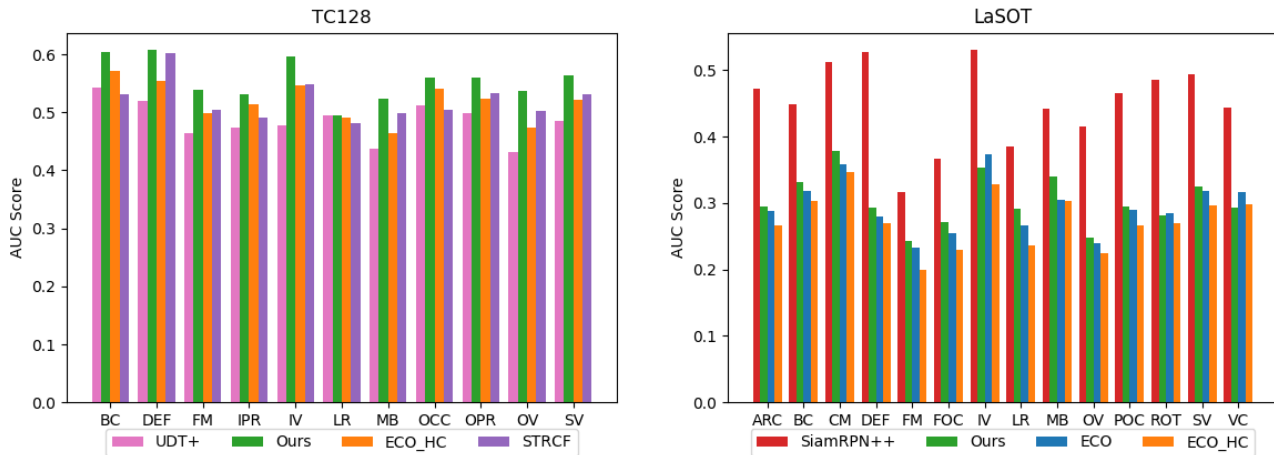


Fig. 11: The area-under-curve (AUC) scores for two datasets, TC128 and LaSOT, under the attribute-based evaluation, where attributes of concern include the aspect ratio change (ARC), background clutter (BC), camera motion (CM), deformation (DEF), fast motion (FM), full occlusion (FOC), in-plane rotation (IPR), illumination variation (IV), low resolution (LR), motion blur (MB), occlusion (OCC), out-of-plane rotation (OPR), out-of-view (OV), partial occlusion (POC), scale variation (SV) and viewpoint change (VC), respectively.

clusion (OCC), out-of-plane rotation (OPR), out-of-view (OV), partial occlusion (POC), scale variation (SV) and viewpoint change (VC). We compare the AUC scores of supervised trackers (e.g., SiamRPN++ and ECO) and unsupervised trackers (e.g., UHP-SOT++, ECO-HC, UDT+ and STRCF) under these attributes in Fig. 11.

We have the following observations. First, among unsupervised trackers, UHP-SOT++ has leading performance in all attributes, which reveals improved robustness from its basic modules and fusion strategy. Second, although ECO utilizes deep features, it is weak in flexible box regression and, as a result, it is outperformed by UHP-SOT++ in handling such deformation and shape changes against LaSOT. In contrast, SiamRPN++ is better than other trackers especially in DEF (deformation), ROT (rotation) and VC (viewpoint change). The superior performance of SiamRPN++ demonstrates the power of its region proposal network (RPN) in generating tight boxes. The RPN inside SiamRPN++ not only improves IoU score but also has the long-term benefit by excluding noisy information. Fourth, supervised trackers perform better in IV (illumination variation) and LR (low resolution) than unsupervised trackers in general. This can be explained by the fact that unsupervised trackers adopt HOG, CN features or other shallow features which do not work well under these attributes. They focus on local structures of the appearance and tend to fail to capture the object when the local gradient or color information is not stable. Finally, even with the feature limitations, UHP-SOT++ still runs second in many attributes against LaSOT because of the stability offered by trajectory prediction and its capability to recover from tracking loss via background motion modeling.

V. EXEMPLARY SEQUENCES AND QUALITATIVE ANALYSIS

After providing quantitative results in Sec. IV, we conduct error analysis on a couple of representative sequences to gain more insights in this section. Several exemplary sequences from LaSOT are shown in Fig. 12, in which SiamRPN++ performs either very well or quite poorly. In the first two sequences, we see the power of accurate box regression contributed by the RPN. In this type of sequences, good trackers can follow the object well. Yet, their poor bounding boxes lead to a low success score. Furthermore, the appearance model would be contaminated by the background information as shown in the second cat example. The appearance model of DCF-based methods learns background texture (rather than follows the cat) gradually. When the box only covers part of the object, it might also miss some object features, resulting in a degraded appearance model. In both scenarios, the long-term performance will drop rapidly. Although UHP-SOT++ allows the aspect ratio change to some extent as seen in the first flag example, its residual map obtained by background motion modeling is still not as effective as the RPN due to lack of semantic meaning. Generally speaking, the performance of UHP-SOT++ relies on the quality of the appearance model and the residual map.

On the other hand, SiamRPN++ is not robust enough to handle a wide range of sequences well. The third example sequence is from video games. SiamRPN++ somehow includes background objects in its box proposals and drifts away from its targets in the presented frames. Actually, these background objects are different from their corresponding target objects in either semantic meaning or local information such as color or texture. The performance of the other three trackers is not affected. We see that they follow the ground truth without

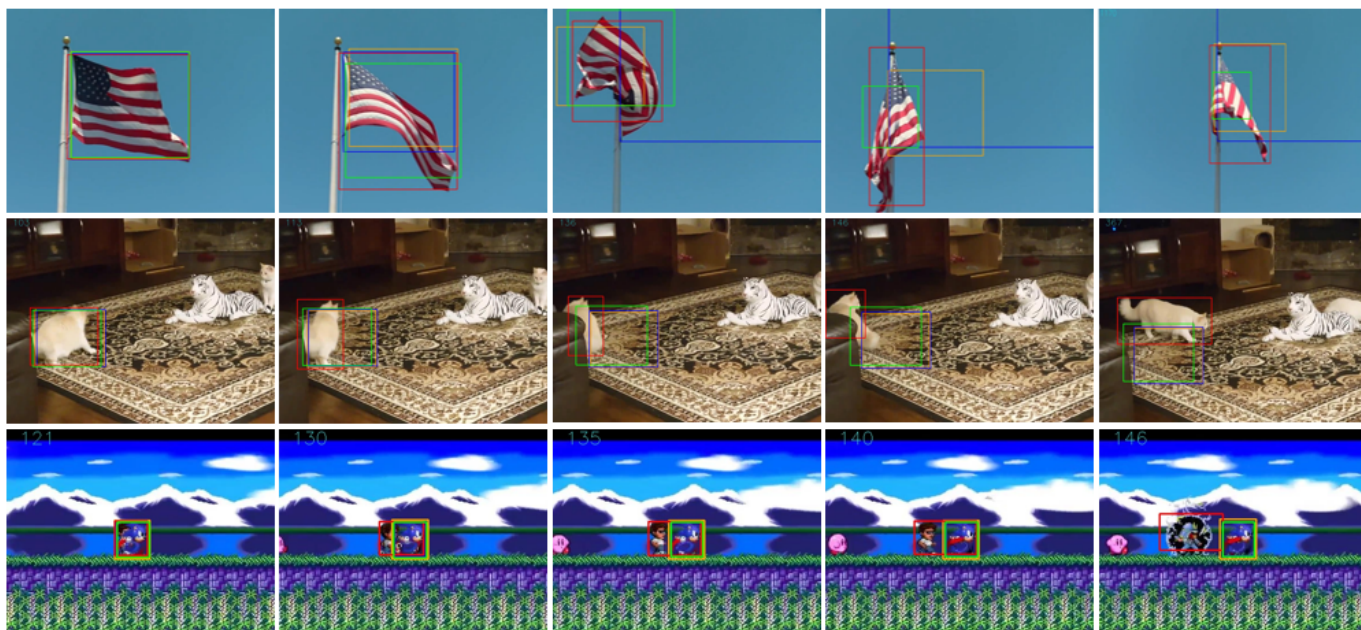


Fig. 12: Qualitative comparison of top runners against the LaSOT dataset, where tracking boxes of SiamRPN++, UHP-SOT++, ECO and ECO-HC are shown in red, green, blue and yellow, respectively. The first two rows show sequences in which SiamRPN++ outperforms others significantly while the last row offers the sequence in which SiamRPN++ performs poorly.



Fig. 13: Illustration of three sequences in which UHP-SOT++ performs the best. The tracking boxes of SiamRPN++, UHP-SOT++, ECO and ECO-HC are shown in red, green, blue and yellow, respectively.

any problem. One explanation is that these video game sequences could be few in the training set and, as a result, SiamRPN++ cannot offer a reliable tracking result for them.

Finally, several sequences in which UHP-SOT++ has the top performance are shown in Fig. 13. In the first cup sequence, all other benchmarking methods lose the target while UHP-SOT++ could go back to the object once the object has obvious motion in the scene. In the second bottle sequence, UHP-SOT++ successfully detects occlusion without making random guesses and the object box trajectory avoids the box to drift away. In contrast, other trackers make ambitious moves without considering the inertia of motion. The third bus sequence is a complicated one that involves several challenges such as full occlusion, scale change and aspect ratio change. UHP-SOT++ is the only one that can recover from tracking loss and provide flexible box predictions. These examples demonstrate the potential of UHP-SOT++ that exploits object and background motion clues across frames effectively.

VI. CONCLUSION AND FUTURE WORK

An unsupervised high-performance tracker, UHP-SOT++, was proposed in this paper. It incorporated two new modules in the STRCF tracker module. They were the background motion modeling module and the object box trajectory modeling module. Furthermore, a novel fusion strategy was adopted to combine proposals from all three modules systematically. It was shown by extensive experimental results on large-scale datasets that UHP-SOT++ can generate robust and flexible object bounding boxes and offer a real-time high-performance tracking solution on resource-limited platforms.

The pros and cons of supervised and unsupervised trackers were discussed. Unsupervised trackers such as UHP-SOT and UHP-SOT++ have the potential in delivering an explainable lightweight tracking solution while maintaining good performance in accuracy. Supervised trackers such as SiamRPN++ benefit from offline end-to-end learning and perform well in general. However, they need to run on GPUs, which is too costly for mobile and edge devices. They may encounter problems in rare samples. Extensive supervision with annotated object boxes is costly. Lack of interpretability could be a barrier for further performance boosting.

Although UHP-SOT++ offers a state-of-the-art unsupervised tracking solution, there is still a performance gap between UHP-SOT++ and SiamRPN++. It is worthwhile to find innovative ways to narrow down the performance gap while keeping its attractive features such as interpretability, unsupervised real-time tracking capability on small devices, etc. as future extension. One idea is to find salient points in the predicted and reference frames individually, develop a way to build their correspondences, and reconstruct the object box in the predicted frame based on its salient points.

REFERENCES

- [1] J. Xing, H. Ai, and S. Lao, "Multiple human tracking based on multi-view upper-body detection and discriminative learning," in *2010 20th International Conference on Pattern Recognition*. IEEE, 2010, pp. 1698–1701.
- [2] J. Janai, F. Güney, A. Behl, A. Geiger *et al.*, "Computer vision for autonomous vehicles: Problems, datasets and state of the art," *Foundations and Trends® in Computer Graphics and Vision*, vol. 12, no. 1–3, pp. 1–308, 2020.
- [3] G. Zhang and P. A. Vela, "Good features to track for visual slam," in *Proceedings of the IEEE conference on computer vision and pattern recognition*, 2015, pp. 1373–1382.
- [4] A. Yilmaz, O. Javed, and M. Shah, "Object tracking: A survey," *Acm computing surveys (CSUR)*, vol. 38, no. 4, pp. 13–es, 2006.
- [5] M. Fiaz, A. Mahmood, S. Javed, and S. K. Jung, "Handcrafted and deep trackers: Recent visual object tracking approaches and trends," *ACM Computing Surveys (CSUR)*, vol. 52, no. 2, pp. 1–44, 2019.
- [6] A. Krizhevsky, I. Sutskever, and G. E. Hinton, "Imagenet classification with deep convolutional neural networks," *Advances in neural information processing systems*, vol. 25, pp. 1097–1105, 2012.
- [7] K. Chatfield, K. Simonyan, A. Vedaldi, and A. Zisserman, "Return of the devil in the details: Delving deep into convolutional nets," *arXiv preprint arXiv:1405.3531*, 2014.
- [8] M. Danelljan, G. Bhat, F. Shahbaz Khan, and M. Felsberg, "Eco: Efficient convolution operators for tracking," in *Proceedings of the IEEE conference on computer vision and pattern recognition*, 2017, pp. 6638–6646.
- [9] M. Danelljan, A. Robinson, F. S. Khan, and M. Felsberg, "Beyond correlation filters: Learning continuous convolution operators for visual tracking," in *European conference on computer vision*. Springer, 2016, pp. 472–488.
- [10] C. Ma, J.-B. Huang, X. Yang, and M.-H. Yang, "Hierarchical convolutional features for visual tracking," in *Proceedings of the IEEE international conference on computer vision*, 2015, pp. 3074–3082.
- [11] Y. Qi, S. Zhang, L. Qin, H. Yao, Q. Huang, J. Lim, and M.-H. Yang, "Hedged deep tracking," in *Proceedings of the IEEE conference on computer vision and pattern recognition*, 2016, pp. 4303–4311.
- [12] N. Wang, W. Zhou, Q. Tian, R. Hong, M. Wang, and H. Li, "Multi-cue correlation filters for robust visual tracking," in *Proceedings of the IEEE conference on computer vision and pattern recognition*, 2018, pp. 4844–4853.
- [13] B. Li, J. Yan, W. Wu, Z. Zhu, and X. Hu, "High performance visual tracking with siamese region proposal network," in *Proceedings of the IEEE conference on computer vision and pattern recognition*, 2018, pp. 8971–8980.
- [14] B. Li, W. Wu, Q. Wang, F. Zhang, J. Xing, and J. Yan, "Siamrpn++: Evolution of siamese visual tracking with very deep networks," in *Proceedings of the IEEE/CVF Conference on Computer Vision and Pattern Recognition*, 2019, pp. 4282–4291.
- [15] X. Lu, C. Ma, B. Ni, X. Yang, I. Reid, and M.-H. Yang, "Deep regression tracking with shrinkage loss," in *Proceedings of the European conference on computer vision (ECCV)*, 2018, pp. 353–369.
- [16] H. Nam and B. Han, "Learning multi-domain convolutional neural networks for visual tracking," in *Proceedings of the IEEE conference on computer vision and pattern recognition*, 2016, pp. 4293–4302.
- [17] S. Pu, Y. Song, C. Ma, H. Zhang, and M.-H. Yang, "Deep attentive tracking via reciprocative learning," *arXiv preprint arXiv:1810.03851*, 2018.
- [18] Y. Song, C. Ma, L. Gong, J. Zhang, R. W. Lau, and M.-H. Yang, "Crest: Convolutional residual learning for visual tracking," in *Proceedings of the IEEE international conference on computer vision*, 2017, pp. 2555–2564.
- [19] L. Bertinetto, J. Valmadre, J. F. Henriques, A. Vedaldi, and P. H. Torr, "Fully-convolutional siamese networks for object tracking," in *European conference on computer vision*. Springer, 2016, pp. 850–865.
- [20] R. Tao, E. Gavves, and A. W. Smeulders, "Siamese instance search for tracking," in *Proceedings of the IEEE conference on computer vision and pattern recognition*, 2016, pp. 1420–1429.
- [21] Z. Zhu, Q. Wang, B. Li, W. Wu, J. Yan, and W. Hu, "Distractor-aware siamese networks for visual object tracking," in *Proceedings of the European Conference on Computer Vision (ECCV)*, 2018, pp. 101–117.

- [22] Q. Wang, Z. Teng, J. Xing, J. Gao, W. Hu, and S. Maybank, "Learning attentions: residual attentional siamese network for high performance online visual tracking," in *Proceedings of the IEEE conference on computer vision and pattern recognition*, 2018, pp. 4854–4863.
- [23] A. He, C. Luo, X. Tian, and W. Zeng, "A twofold siamese network for real-time object tracking," in *Proceedings of the IEEE Conference on Computer Vision and Pattern Recognition*, 2018, pp. 4834–4843.
- [24] N. Wang, W. Zhou, J. Wang, and H. Li, "Transformer meets tracker: Exploiting temporal context for robust visual tracking," in *Proceedings of the IEEE/CVF Conference on Computer Vision and Pattern Recognition*, 2021, pp. 1571–1580.
- [25] X. Chen, B. Yan, J. Zhu, D. Wang, X. Yang, and H. Lu, "Transformer tracking," in *Proceedings of the IEEE/CVF Conference on Computer Vision and Pattern Recognition*, 2021, pp. 8126–8135.
- [26] D. S. Bolme, J. R. Beveridge, B. A. Draper, and Y. M. Lui, "Visual object tracking using adaptive correlation filters," in *2010 IEEE computer society conference on computer vision and pattern recognition*. IEEE, 2010, pp. 2544–2550.
- [27] J. F. Henriques, R. Caseiro, P. Martins, and J. Batista, "High-speed tracking with kernelized correlation filters," *IEEE transactions on pattern analysis and machine intelligence*, vol. 37, no. 3, pp. 583–596, 2014.
- [28] M. Danelljan, G. Hager, F. Shahbaz Khan, and M. Felsberg, "Convolutional features for correlation filter based visual tracking," in *Proceedings of the IEEE international conference on computer vision workshops*, 2015, pp. 58–66.
- [29] M. Danelljan, G. Häger, F. S. Khan, and M. Felsberg, "Discriminative scale space tracking," *IEEE transactions on pattern analysis and machine intelligence*, vol. 39, no. 8, pp. 1561–1575, 2016.
- [30] L. Bertinetto, J. Valmadre, S. Golodetz, O. Miksik, and P. H. Torr, "Staple: Complementary learners for real-time tracking," in *Proceedings of the IEEE conference on computer vision and pattern recognition*, 2016, pp. 1401–1409.
- [31] J. Valmadre, L. Bertinetto, J. Henriques, A. Vedaldi, and P. H. Torr, "End-to-end representation learning for correlation filter based tracking," in *Proceedings of the IEEE conference on computer vision and pattern recognition*, 2017, pp. 2805–2813.
- [32] F. Li, C. Tian, W. Zuo, L. Zhang, and M.-H. Yang, "Learning spatial-temporal regularized correlation filters for visual tracking," in *Proceedings of the IEEE conference on computer vision and pattern recognition*, 2018, pp. 4904–4913.
- [33] M. Danelljan, G. Hager, F. Shahbaz Khan, and M. Felsberg, "Learning spatially regularized correlation filters for visual tracking," in *Proceedings of the IEEE international conference on computer vision*, 2015, pp. 4310–4318.
- [34] N. Wang, Y. Song, C. Ma, W. Zhou, W. Liu, and H. Li, "Unsupervised deep tracking," in *Proceedings of the IEEE/CVF Conference on Computer Vision and Pattern Recognition*, 2019, pp. 1308–1317.
- [35] N. Wang, W. Zhou, Y. Song, C. Ma, W. Liu, and H. Li, "Unsupervised deep representation learning for real-time tracking," *International Journal of Computer Vision*, vol. 129, no. 2, pp. 400–418, 2021.
- [36] Q. Wu, J. Wan, and A. B. Chan, "Progressive unsupervised learning for visual object tracking," in *Proceedings of the IEEE/CVF Conference on Computer Vision and Pattern Recognition*, 2021, pp. 2993–3002.
- [37] Z. Zhou, H. Fu, S. You, C. C. Borel-Donohue, and C.-C. J. Kuo, "Uhp-sot: An unsupervised high-performance single object tracker," *arXiv preprint arXiv:2110.01812*, 2021.
- [38] Y. Wu, J. Lim, and M.-H. Yang, "Object tracking benchmark," *IEEE Transactions on Pattern Analysis and Machine Intelligence*, vol. 37, no. 9, pp. 1834–1848, 2015.
- [39] M. Danelljan, F. Shahbaz Khan, M. Felsberg, and J. Van de Weijer, "Adaptive color attributes for real-time visual tracking," in *Proceedings of the IEEE Conference on Computer Vision and Pattern Recognition*, 2014, pp. 1090–1097.
- [40] K. Hariharakrishnan and D. Schonfeld, "Fast object tracking using adaptive block matching," *IEEE transactions on multimedia*, vol. 7, no. 5, pp. 853–859, 2005.
- [41] A. Aggarwal, S. Biswas, S. Singh, S. Sural, and A. K. Majumdar, "Object tracking using background subtraction and motion estimation in mpeg videos," in *Asian Conference on Computer Vision*. Springer, 2006, pp. 121–130.
- [42] P. Liang, E. Blasch, and H. Ling, "Encoding color information for visual tracking: Algorithms and benchmark," *IEEE Transactions on Image Processing*, vol. 24, no. 12, pp. 5630–5644, 2015.
- [43] M. Mueller, N. Smith, and B. Ghanem, "A benchmark and simulator for uav tracking," in *European conference on computer vision*. Springer, 2016, pp. 445–461.
- [44] H. Fan, L. Lin, F. Yang, P. Chu, G. Deng, S. Yu, H. Bai, Y. Xu, C. Liao, and H. Ling, "Lasot: A high-quality benchmark for large-scale single object tracking," in *Proceedings of the IEEE/CVF Conference on Computer Vision and Pattern Recognition*, 2019, pp. 5374–5383.
- [45] L. Alan, T. Vojít, L. Čehovin, J. Matas, and M. Kristan, "Discriminative correlation filter tracker with channel and spatial reliability," *International Journal of Computer Vision*, vol. 126, no. 7, pp. 671–688, 2018.
- [46] C. Ma, X. Yang, C. Zhang, and M.-H. Yang, "Long-term correlation tracking," in *Proceedings of the IEEE conference on computer vision and pattern recognition*, 2015, pp. 5388–5396.